Self-Assembled Nanostructures

DOI: 10.1002/ange.201300834

Bottom-Up-Assembled Nanostar Colloids of Gold Cores and Tubes Derived From Tobacco Mosaic Virus**

*Fabian J. Eber, Sabine Eiben, Holger Jeske, and Christina Wege**

Ordered biogenic molecular complexes, such as filamentous, tubular, or spherical virus particles, expose a high density of regularly arranged functional groups on their surfaces, which allows for the coupling of further functional groups or for genetic modification.[1] Some of them are non-pathogenic to humans, stable under a wide range of conditions, and can be produced in suitable hosts at high yields. In combination with the high surface-to-volume ratio of the nanostructures, this has led to their use as versatile biological scaffolds,[2] and as capture elements in sensor devices or diagnostic tools.[3] Their controlled integration with inorganic components still remains a challenge, but is essential for nanotechnology advancements enabling, for example, a physical read out of biological interactions. Inorganic nanoparticles in this context may be magnetic, fluorescent, plasmonic, or electrically conductive, properties which are not only important for mediating signal transduction by optical methods or electrical fluxes, but also for enabling bioseparation procedures.[4] However, conventional methods have thus far typically made use of relatively simply coated surfaces of inorganic particles such as metal beads, which often induce unpredictable folding of adsorbed capture proteins, which leads to significant losses of activity, and offers only limited surface area.[5] Novel composite materials, which combine the advantages of densely exposed coupling groups on high soft-matter surface-area nanostructures with robust inorganic carrier beads may therefore be a key to substantially improved separation and detection performance, namely for the immobilization of active protein species. Accordingly, an initial study on suitable architectures recently evaluated the capacity of pre-assembled M13 bacteriophages to modify magnetic microparticles.[6] However, the coupling of the nucleoprotein fibers to the metal cores was not very efficient: different methods achieved a maximum surface enhancement factor of less than 1.1. We have investigated an alternative production route for highly defined virus–inorganic nanoparticle adducts with a multitude of readily protruding proteinaceous carrier templates, based on the stiff tobacco mosaic virus (TMV).

Whereas a number of studies have focused on the site-specific equipment of individual plant or bacterial viruses with one or more metal beads,[7] we describe here an RNA-directed bottom-up assembly procedure yielding bioinorganic hybrid nanostars with numerous virus-derived arms, and thus an exceptionally high and tunable ratio of protein surface area to the metal cores. This was achieved by encapsidating immobilized RNA on gold beads with TMV coat protein (CP). The specificity of RNA hybridization to oligodeoxynucleotides exposed on gold nanoparticles of different diameters allowed the simultaneous fabrication of star colloids with distinct pre-determined arm-length distributions in single-batch processes.

TMV is a nanotubular plant virus with an outer diameter of 18 nm, an inner diameter of 4 nm and 300 nm length. The tube is formed by about 2130 identical copies of CP, which encapsidate a single genomic RNA of 6395 nucleotides (nts) in infected plant cells. TMV CP may also package non-viral RNA if expressed in plant, yeast, or bacterial cells.[8] In vitro, TMV CP self-assembles under appropriate conditions to yield tubes, spheres, or disk-like aggregates.[9] RNA-mediated control over the self-assembly of TMV CP determines the length and, thereby, may alter the chemical or physical properties of the tube-shaped particles formed in vitro.[10] TMV RNA both initiates and limits the bidirectional growth of the helical protein coat, which integrates and protects the nucleic acid. A specific interaction of an internal stem–loop-forming RNA sequence, the origin of assembly (OA), with a two-layered ring-shaped multimer of 34 TMV CP subunits (a 20S disk) triggers the self-assembly: transformation of the CP aggregate into a helical "lockwasher" inserts the RNA strand between the protein layers and thereby draws the 5′ portion of the RNA into the nascent tubular complex. Further disks are then added serially, to build a continuous protein helix through conformational switching, which encapsidates the RNA until its 5′ terminus is reached. The 3′ terminus of the RNA is packed at a slower rate by the addition of only trimeric or monomeric CP subunits (A protein). We were recently able to demonstrate that this mechanism is not only suitable to grow nanorods with programmed longitudinal domains,[11] but also to interconnect the biomolecular templates with a synthetic environment: TMV-like rods were assembled bottom-up on planar silica substrates with RNA linked at its 3′ end to an oligonucleotide anchor on the surface, but the surface coverage was difficult to control.[12]

To obtain densely packed free-floating nanotube ensembles in this study, gold nanospheres (AuNPs) were functionalized with oligonucleotides,[13] which are readily accessible

[*] Dr. F. J. Eber, Dr. S. Eiben, Prof. H. Jeske, Prof. C. Wege
Department of Molecular Biology and Plant Virology, Institute of Biology, University of Stuttgart
Pfaffenwaldring 57, 70569 Stuttgart (Germany)
E-mail: christina.wege@bio.uni-stuttgart.de
Homepage: http://www.uni-stuttgart.de/bio/bioinst/molbio

[**] We acknowledge the Baden-Wuerttemberg-Stiftung (KFN) and the DFG (SPP1165) for financial support and thank Conny Kocher for TEM analyses, Sigrid Kober for TMV preparations, and Sven Degenhard, Anan Kadri, and Fania Geiger for fruitful discussions and for providing some of their primer stocks.

Supporting information for this article is available on the WWW under http://dx.doi.org/10.1002/anie.201300834.

Table 1: Characteristics of the different RNA molecules, of their 3′ end sequences, and of the capture oligomers used in this study.

RNA name	3′ End sequence						Capture oligomer		
	Length [nts]	Origin	Position[a]	Length [nts]	Name	Sequence	Name	G/C [%]	T_m[b] [°C]
RNA_s-SeqA	2253	pGEM-T	472	35	SeqA	5′-...CCACAGAAUCAGGGGAUAACGCAGGAAAGAACAUG-3′	HS-T_{15}-SeqĀ	49	84
RNA_s-SeqB	1989	TMV	6249[c]	31	SeqB	5′-...GAUUGUGUCCGUAAUCACACGUGGUGCGUAC-3′	HS-T_{15}-SeqB̄	52	72
RNA_l-SeqB	7025	TMV	6249[c]	31	SeqB	5′-...GAUUGUGUCCGUAAUCACACGUGGUGCGUAC-3′	HS-T_{15}-SeqB̄	52	72

[a] Position in base pairs or nucleotides, respectively. [b] Nearest neighbor calculation[16] with parameters for RNA–DNA hybrids;[17] monovalent salt correction of 0.85 M,[18] oligonucleotide concentration of 0.15 nM. [c] See [15].

for hybridization of nucleic acids.[14] AuNPs were first functionalized through thiol–Au bonds with the deoxyoligonucleotide HS-T_{15}-SeqĀ, which is reverse complementary to the 3′ end of the RNA_s-SeqA, but not to RNA_s-SeqB, which served as a control (for details of abbreviations and sequence characteristics, see Table 1). To adjust the surface density of assembly-inducing RNA per nanobead, one end of OA-containing RNAs was hybridized to the immobilized DNA under variable conditions. The effects of the resulting RNA surface concentrations on the assembly of TMV CP were investigated.

After molecular hybridization of the RNA to the DNA, and purification of the nucleic acid–gold complexes, assembly-competent TMV CP was added under conditions promoting RNA-guided tube growth. Transmission electron microscopy (TEM) revealed efficient formation of star-shaped architectures for RNA_s-SeqA, with gold nanoparticles as cores and numerous straight arms of TMV-like nanotubes (Figure 1a and c). The reaction went to completion, with all gold beads that were initiated with DNA experiencing nucleation events. The density of nanotubes nearly reached surface saturation, without displacement of the non-covalently immobilized RNA from the solid support. Importantly, nanostars were not observed if the DNA-modified gold particles were incubated with preassembled nanotubes (Figure 1e and f), excluding nonspecific binding of the ends of the nucleoprotein tubes to the beads. Moreover, no nanostars were generated upon the use of gold particles treated with control RNA_s-SeqB in the hybridization step (Figure 1b and d), which lacked complementarity to the DNA oligomers on the AuNPs. Hence, interactions between RNA scaffolds and DNA targets were fully sequence specific.

To vary and regulate the number of arms on the gold cores, different amounts of RNA per AuNP were used for hybridization. The RNA load on two species of AuNPs of different sizes increased with the concentration of RNA applied for hybridization, as indicated by decreased mobility of the complexes during native agarose gel electrophoresis (Figure 2a). Their distinct RNA load was also reflected by the number of arms of the resulting nanostars after assembly of TMV CP (Figure 2b,c), with up to about 15 arms for AuNPs of 10 nm diameter and up to about 30 arms for AuNPs of 50 nm diameter.

Taking into account the surface area of the AuNPs (314 nm^2 for 10 nm diameter NPs, 7854 nm^2 for 50 nm diameter NPs), the spacing of adjacent RNA anchor points of nanotubes on a single AuNP amounts to only about 5 nm or 16 nm, respectively. As we observed the structures as

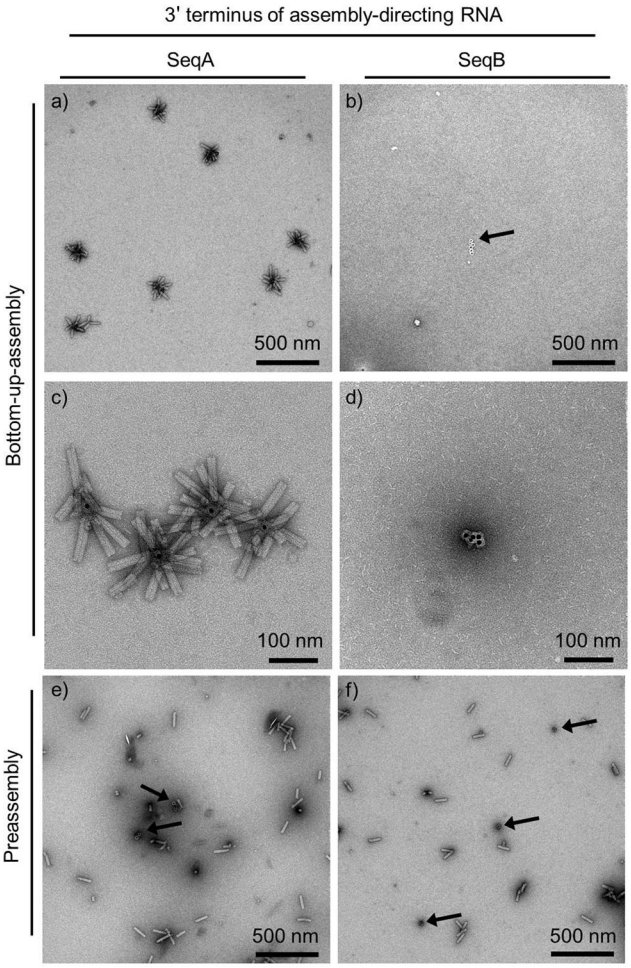

Figure 1. Generation of nanostars after site-specific hybridization of TMV-derived synthetic RNA_s-SeqA to gold-nanoparticle-bound oligonucleotides HS-T_{15}-SeqĀ, followed by RNA-guided assembly of viral CP (a, c). As control for non-specific RNA binding, RNA_s-SeqB lacking the targeting sequence was used (b, d). RNA was either subjected to CP assembly before incubation with the gold nanoparticles, denoted as preassembly (e and f), which acts as a control for unspecific nanotube binding, or after its hybridization to the gold nanoparticles, denoted as bottom-up assembly (a–d). Samples were negatively stained and visualized by TEM. Arrows indicate free gold nanoparticles.

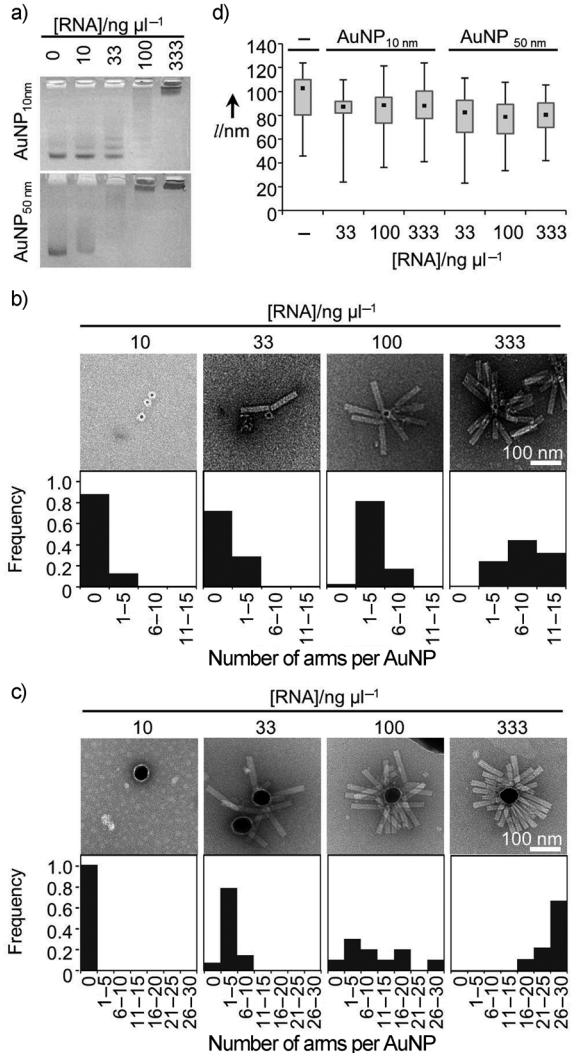

Figure 2. Influence of different RNA_s-SeqA surface concentrations and AuNP diameters on nanostar formation. a) Native gel electrophoresis of oligonucleotide-equipped AuNPs with different RNA loads achieved by varying the concentration of RNA per AuNP equivalent in the hybridization reaction. Purified products were separated in a 1% agarose gel. b) and c) TEM images (upper row) and distribution (lower row) of nanostar types arising from self-assembly of TMV CP on 10 nm (b) and 50 nm (c) AuNPs with different RNA surface concentrations. d) Comparison of the length (*l*) distributions of the arms of the nanostars on AuNPs of different diameters and of different RNA surface concentrations. As a reference, the length distribution of assembly products directed by free RNA_s-SeqA (2253 nts in length) is provided (–); median values (■), upper and lower quartiles (gray boxes); error bars indicate the maximum and minimum values.

a projection in two dimensions, we underestimated the amount of nanotubes on the larger AuNPs, which resulted in a higher apparent distance. The dense packing of TMV-like tubes leads to a 240-fold increase in surface area for the 10 nm AuNP hybrids with 15 arms, and its surface-to-volume ratio approaches that of the cylindrical arms ($2.3 \times 10^8\ m^2\,m^{-3}$). The surface concentration of nucleoprotein tubes obtained with our bottom-up strategy (47700 particles per μm^2) is a huge improvement, taking into account that the deposition of preassembled M13 phages on magnetic particles resulted in an average surface concentration of only four particles per μm^2.[6]

Immobilization of scaffolding RNAs on planar silica supports led to an assembly of rods shorter than those grown on the same RNAs in solution.[12a] Correspondingly, the immobilized RNA of 2253 nts (RNA_s-SeqA) yielded only 84 nm long nucleoprotein arms on the gold beads, compared to 103 nm long nanotubes formed in solution (Figure 2c; median values). This deviation indicates that about 400 nts were not encapsidated, a value independent of the RNA surface concentration on the gold cores. Tube lengths did not differ significantly between AuNPs of 10 nm and 50 nm diameter, which indicates that the effect also does not correlate with the surface curvature to a detectable extent.

The difference was more pronounced for longer RNA. AuNPs were conjugated with the oligonucleotide HS-T_{15}-SeqB̄, which bound the 7025 nts long RNA_l-SeqB in a concentration-dependent manner similar to the first combination of oligonucleotide and RNA, as confirmed by gel-mobility assays (Figure 3a). For unknown reasons, this particular AuNP preparation already showed two distinct bands during electrophoresis before oligonucleotide conjugation (not shown).

After RNA-directed assembly of TMV CP (Figure 3b), the rod length was decreased from 315 nm for free RNA to a median value of 110 nm for immobilized RNA; longer arms were formed only sporadically. The reduction of nanotube length was independent of the surface concentration of RNA (Figure 3c). In summary, the growth of TMV-like arms of around 100 nm length was possible in close vicinity to each other, without further interference with their final size. Long RNAs did not efficiently scaffold proportionally elongated surface-linked tubes. We conclude that the characteristically decreased length of bottom-up-assembled nucleoprotein tubes does not mainly result from steric hindrance between adjacently growing nucleoprotein tubes. We rather suspect that shortened tubes result from a combination of both incomplete 3′-terminal packaging of RNA close to the liquid–solid interface, and premature 5′ termination. The latter may apply more frequently to long RNAs, if yet unencapsidated stretches cannot be drawn through nascent tube portions, for example, due to interactions with the support or locally accumulated CP oligomers.

With the two different AuNP sizes functionalized with distinct oligonucleotides, and the two different lengths of scaffold RNA, the specificity of hybridization was further confirmed by mixed batch approaches (see the Supporting Information for details). This indicates the possibility of configuring the nanostar structures in a sequence-specific manner, which provides opportunities for multiplexing approaches and might also serve as basis for the development of cost- and effort-efficient one-pot production routes.

The experiments demonstrate for the first time that bottom-up self-assembly of TMV CP tubes guided by immobilized RNA can occur on inorganic nanoparticles with very high surface concentrations. We first bound the assembly-triggering RNA on gold beads to generate a complex composite scaffold for the subsequent directed self-organization of TMV CP. No restriction on the nucleoprotein tube

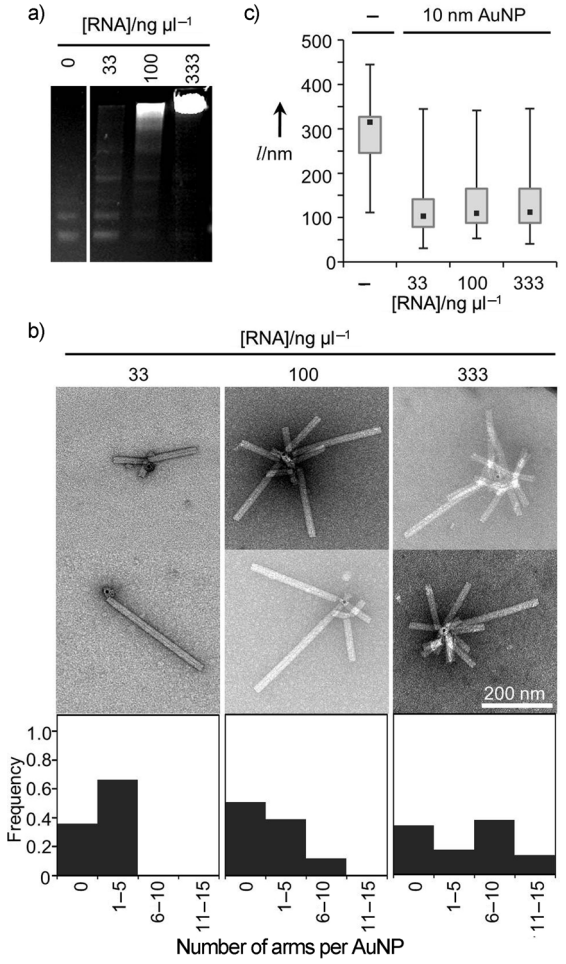

Figure 3. Nanostar formation directed by RNA-equipped AuNPs with long RNA molecules (RNA_I-SeqB, 7025 nts). a) Gel electrophoretic analysis of hybridization products. Different concentrations of RNA were used to achieve different surface concentrations of RNA on the AuNPs. The purified hybridization products were separated in a 1% agarose gel and documented under UV light after ethidium bromide staining. b) TEM images and distribution of nanostar types arising from self-assembly of TMV CP directed by RNA-equipped AuNPs. c) Comparison of the lengths of the arms of the nanostars that arise at different RNA densities. The lengths of assembly products of TMV CP directed by free RNA_I-SeqB are provided as a control; median values (■), upper and lower quartiles (gray boxes); error bars indicate the maximum and minimum values.

surface density was imposed by the assembly process. In contrast, the surface coverage of TMV-like rods grown on flat substrates through similar approaches only locally achieved saturation sensitive to control.[12]

The star-like bio-inorganic hybrid architectures might be developed further into high-protein-surface-area carrier colloids, for example, to densely expose captured molecules for magnetic bioseparation or cytometric bead arrays.[19] Notably, a twofold specificity could be achieved with this new method: 1) only one specific end of the nanotubes was addressed, and 2) only nanospheres bearing nucleic acids complementary to the assembly-directing RNA were modified. The free energy released upon the nucleoprotein self-organization process did not separate the DNA/RNA hybrids; upon storage at 4 °C, the nanostars were stable for at least several days. In comparison to reported virus-derived composites,[7,20] among them a singular type of radial TMV fragment arrays formed inside nascent silica nanoparticles, these hybrid virus–metal nanoarchitectures differ substantially:[20] 1) Single inorganic cores were equipped with multiple freely protruding nucleoprotein arms 2) in a tunable way 3) by bottom-up in vitro self-assembly. This was achieved by selectively addressing one end of a scaffolding RNA, another unique aspect in nanoparticle functionalization, which may open new routes towards multiplexing during the fabrication of complex functional nanoassemblies.

In conclusion, the tightly controlled combination of an inorganic nanoparticle with the precisely organized biomolecular complex of a virion has yielded a novel generation of large ordered multicomponent nanocomposites.

Received: January 30, 2013
Published online: June 12, 2013

Keywords: nanostructures · proteins · RNA · self-assembly · tobacco mosaic virus

[1] a) A. Kadri, E. Maiss, N. Amsharov, A. M. Bittner, S. Balci, K. Kern, H. Jeske, C. Wege, *Virus Res.* **2011**, *157*, 35–46; b) N. F. Steinmetz, T. Lin, G. P. Lomonossoff, J. E. Johnson, *Curr. Top. Microbiol. Immunol.* **2009**, *327*, 23–58.

[2] a) M. Fischlechner, E. Donath, *Angew. Chem.* **2007**, *119*, 3246–3255; *Angew. Chem. Int. Ed.* **2007**, *46*, 3184–3193; b) C. M. Soto, B. R. Ratna, *Curr. Opin. Biotechnol.* **2010**, *21*, 426–438; c) E. Dujardin, C. Peet, G. Stubbs, J. N. Culver, S. Mann, *Nano Lett.* **2003**, *3*, 413–417; d) K. M. Bromley, A. J. Patil, A. W. Perriman, G. Stubbs, S. Mann, *J. Mater. Chem.* **2008**, *18*, 4796–4801; e) M. Young, D. Willits, M. Uchida, T. Douglas, *Annu. Rev. Phytopathol.* **2008**, *46*, 361–384; f) S. Werner, S. Marillonnet, G. Hause, V. Klimyuk, Y. Gleba, *Proc. Natl. Acad. Sci. USA* **2006**, *103*, 17678–17683.

[3] a) H. Seok, T. H. Park, *Biotechnol. J.* **2011**, *6*, 1310–1316; b) J. H. Lee, J. S. Kim, J. S. Park, W. Lee, K. E. Lee, S. S. Han, K. B. Lee, J. Lee, *Adv. Funct. Mater.* **2010**, *20*, 2004–2009; c) R. de La Rica, C. Pejoux, H. Matsui, *Adv. Funct. Mater.* **2011**, *21*, 1018–1026.

[4] a) C. Fitzgerald, M. Collins, S. van Duyne, M. Mikoleit, T. Brown, P. Fields, *J. Clin. Microbiol.* **2007**, *45*, 3323–3334; b) S. Schrittwieser, F. Ludwig, J. Dieckhoff, K. Soulantica, G. Viau, L. M. Lacroix, S. M. Lentijo, R. Boubekri, J. Maynadie, A. Huetten, H. Brueckl, J. Schotter, *ACS Nano* **2012**, *6*, 791–801; c) G. R. Souza, D. R. Christianson, F. I. Staquicini, M. G. Ozawa, E. Y. Snyder, R. L. Sidman, J. H. Miller, W. Arap, R. Pasqualini, *Proc. Natl. Acad. Sci. USA* **2006**, *103*, 1215–1220; d) A. S. Blum, C. M. Soto, K. E. Sapsford, C. D. Wilson, M. H. Moore, B. R. Ratna, *Biosens. Bioelectron.* **2011**, *26*, 2852–2857.

[5] a) Z. J. Deng, M. T. Liang, M. Monteiro, I. Toth, R. F. Minchin, *Nat. Nanotechnol.* **2011**, *6*, 39–44; b) H. Pan, M. Qin, W. Meng, Y. Cao, W. Wang, *Langmuir* **2012**, *28*, 12779–12787; c) W. Shang, J. H. Nuffer, J. S. Dordick, R. W. Siegel, *Nano Lett.* **2007**, *7*, 1991–1995; d) A. A. Vertegel, R. W. Siegel, J. S. Dordick, *Langmuir* **2004**, *20*, 6800–6807.

[6] J. Muzard, M. Platt, G. U. Lee, *Small* **2012**, *8*, 2403–2411.

[7] a) S. Balci, K. Noda, A. M. Bittner, A. Kadri, C. Wege, H. Jeske, K. Kern, *Angew. Chem.* **2007**, *119*, 3210–3212; *Angew. Chem. Int. Ed.* **2007**, *46*, 3149–3151; b) K. T. Nam, D. W. Kim, P. J. Yoo, C. Y. Chiang, N. Meethong, P. T. Hammond, Y. M. Chiang, A. M.

Belcher, *Science* **2006**, *312*, 885 – 888; c) N. F. Steinmetz, A. Bize, K. C. Findlay, G. P. Lomonossoff, M. Manchester, D. J. Evans, D. Prangishvili, *Adv. Funct. Mater.* **2008**, *18*, 3478 – 3486; d) T. Ueno, T. Koshiyama, T. Tsuruga, T. Goto, S. Kanamaru, F. Arisaka, Y. Watanabe, *Angew. Chem.* **2006**, *118*, 4620 – 4624; *Angew. Chem. Int. Ed.* **2006**, *45*, 4508 – 4512; e) L. Torrance, I. A. Andreev, R. Gabrenaite-Verhovskaya, G. Cowan, K. Makinen, M. E. Taliansky, *J. Mol. Biol.* **2006**, *357*, 1 – 8.

[8] A. Kadri, C. Wege, H. Jeske, *J. Virol. Methods* **2013**, *189*, 328 – 340.

[9] a) J. Atabekov, N. Nikitin, M. Arkhipenko, S. Chirkov, O. Karpova, *J. Gen. Virol.* **2011**, *92*, 453 – 456; b) M. A. Bruckman, C. M. Soto, H. McDowell, J. L. Liu, B. R. Ratna, K. V. Korpany, O. K. Zahr, A. S. Blum, *ACS Nano* **2011**, *5*, 1606 – 1616; c) M. Endo, M. Fujitsuka, T. Majima, *Chem. Eur. J.* **2007**, *13*, 8660 – 8666.

[10] a) P. J. G. Butler, *Philos. Trans. R. Soc. London Ser. B* **1999**, *354*, 537 – 550; b) Y. Okada, *Adv. Biophys.* **1986**, *22*, 95 – 149; c) Z. Wu, A. Mueller, S. Degenhard, S. E. Ruff, F. Geiger, A. M. Bittner, C. Wege, C. E. Krill 3rd, *ACS Nano* **2010**, *4*, 4531 – 4538; d) A. Mueller, A. Kadri, H. Jeske, C. Wege, *J. Virol. Methods* **2010**, *166*, 77 – 85; e) J. M. Rego, J. H. Lee, D. H. Lee, H. Yi, *Biotechnol. J.* **2013**, *8*, 237 – 246.

[11] F. C. Geiger, F. J. Eber, S. Eiben, A. Mueller, H. Jeske, J. P. Spatz, C. Wege, *Nanoscale* **2013**, *5*, 3808 – 3816.

[12] a) A. Mueller, F. J. Eber, C. Azucena, A. Petershans, A. M. Bittner, H. Gliemann, H. Jeske, C. Wege, *ACS Nano* **2011**, *5*, 4512 – 4520; b) C. Azucena, F. J. Eber, V. Trouillet, M. Hirtz, S. Heissler, M. Franzreb, H. Fuchs, C. Wege, H. Gliemann, *Langmuir* **2012**, *28*, 14867 – 14877.

[13] L. M. Demers, C. A. Mirkin, R. C. Mucic, R. A. Reynolds III, R. L. Letsinger, R. Elghanian, G. Viswanadham, *Anal. Chem.* **2000**, *72*, 5535 – 5541.

[14] D. A. Giljohann, D. S. Seferos, W. L. Daniel, M. D. Massich, P. C. Patel, C. A. Mirkin, *Angew. Chem.* **2010**, *122*, 3352 – 3366; *Angew. Chem. Int. Ed.* **2010**, *49*, 3280 – 3294.

[15] P. Goelet, G. P. Lomonossoff, P. J. G. Butler, M. E. Akam, M. J. Gait, J. Karn, *Proc. Natl. Acad. Sci. USA* **1982**, *79*, 5818 – 5822.

[16] K. J. Breslauer, R. Frank, H. Blocker, L. A. Marky, *Proc. Natl. Acad. Sci. USA* **1986**, *83*, 3746 – 3750.

[17] N. Sugimoto, S. Nakano, M. Katoh, A. Matsumura, H. Nakamuta, T. Ohmichi, M. Yoneyama, M. Sasaki, *Biochemistry* **1995**, *34*, 11211 – 11216.

[18] a) R. Owczarzy, B. G. Moreira, Y. You, M. A. Behlke, J. A. Walder, *Biochemistry* **2008**, *47*, 5336 – 5353; b) R. Owczarzy, Y. You, B. G. Moreira, J. A. Manthey, L. Huang, M. A. Behlke, J. A. Walder, *Biochemistry* **2004**, *43*, 3537 – 3554.

[19] a) T. L. Maury, K. E. Ottow, J. Brask, J. Villadsen, T. J. Hobley, *Biotechnol. J.* **2012**, *7*, 909 – 918; b) H. Y. Hsu, T. O. Joos, H. Koga, *Electrophoresis* **2009**, *30*, 4008 – 4019.

[20] C. E. Fowler, W. Shenton, G. Stubbs, S. Mann, *Adv. Mater.* **2001**, *13*, 1266 – 1269.

[21] T. A. Taton, *Curr. Protoc. Nucleic Acid Chem.* **2002**, 12.2.1 – 12.2.12.

[22] M. P. Weiner, G. L. Costa, W. Schoettlin, J. Cline, E. Mathur, J. C. Bauer, *Gene* **1994**, *151*, 119 – 123.

[23] a) H. Fraenkel-Conrat, *Virology* **1957**, *4*, 1 – 4; b) H. Fraenkel-Conrat, R. C. Williams, *Proc. Natl. Acad. Sci. USA* **1955**, *41*, 690 – 698; c) G. V. Gooding, T. T. Hebert, *Phytopathology* **1967**, *57*, 1285.

[24] W. K. Kegel, P. van der Schoot, *Biophys. J.* **2006**, *91*, 1501 – 1512.

[25] W. S. Rasband, ImageJ, Program for image processing, US National Institutes of Health, Bethesda, Maryland, USA, 1.43 ed., **1997 – 2010**.

